Applied Science and Engineering Progress, Vol. 20, No. 4, 2027, 8324

Research Article

Water Transport and Swelling Kinetics in NaOH-Saponified Chitosan-g-poly(acrylic acid) Superabsorbent Hydrogels: Model Discrimination and Phenomenological Interpretation

Dimas Prasetyo, Rahmayetty and Jayanudin*
Master of Chemical Engineering, Faculty of Engineering, Universitas Sultan Ageng Tirtayasa, Jl. Raya Jakarta Km 4 Serang, Indonesia

Endarto Yudo Wardhono, Widya Ernayati Kosimaningrum and Rudi Hartono
Chemical Engineering Department, Faculty of Engineering, Universitas Sultan Ageng Tirtayasa, Jalan Jenderal Sudirman km.3 Cilegon, Indonesia

* Corresponding author. E-mail: jayanudin@untirta.ac.id DOI: 10.14416/j.asep.2026.09.013
Received: 9 July 2026; Revised: 9 August 2026; Accepted: 24 August 2026; Published online: 18 September 2026

Abstract
This study reanalyzes the time-dependent swelling data of NaOH-saponified chitosan-graft-poly(acrylic acid) (Cs-g-PAA) superabsorbent hydrogels using complementary empirical, diffusional, and relaxation-based models. Five formulations differed in the degree of acrylic acid neutralization and nominal N,N′-methylenebisacrylamide (MBA) loading. The Schott, Peleg, Weibull, and Voigt models described the complete swelling-ratio profiles, whereas the Ritger–Peppas model was restricted to the initial fractional-uptake region, and the mixed diffusion–relaxation model provided a phenomenological partitioning of two kinetic contributions. Cs-g-PAA-4, prepared at 50% neutralization and with 0.015 g MBA, showed the highest swelling capacity. This result is associated with the lower nominal crosslinker loading but does not independently establish the crosslink density. Statistical indicators were interpreted only within comparable response-variable and data-range frameworks. The mixed model provided high fitting accuracy for most formulations, whereas the Weibull model adequately described the nonlinear swelling profile of Cs-g-PAA-4. These fits support, but do not directly prove, contributions from water transport and time-dependent network rearrangement. The conclusions are limited to the investigated Cs-g-PAA system in distilled water at 27 ± 1 °C.

Keywords: Chitosan-graft-poly(acrylic acid), Model discrimination, Phenomenological modeling, Swelling kinetics, Water transport

1 Introduction

Superabsorbent polymers (SAPs) are three-dimensional hydrophilic networks capable of absorbing and retaining large amounts of water or aqueous fluids without dissolving. Due to their high swelling capacity, water retention ability, and tunable physicochemical properties, SAPs are widely used in agriculture, hygiene products, biomedical materials, controlled-release systems, wastewater treatment, and environmental engineering [1-3]. However, many conventional synthetic SAPs are petroleum-based and poorly biodegradable, encouraging the development of bio-based superabsorbent hydrogels with high water uptake, controllable swelling kinetics, and predictable transport behavior.

Chitosan is a promising natural polymer for sustainable hydrogel development because its amino and hydroxyl groups support hydrogen bonding, grafting reactions, ionic interactions, and water–polymer interactions. Although chitosan-based hydrogels are biodegradable, biocompatible, non-toxic, and structurally versatile [4], native chitosan generally has lower swelling capacity than polyacrylate-based superabsorbents. Grafting acrylic acid onto chitosan is therefore an effective strategy to combine the environmental advantages of chitosan with the high water absorption ability of poly(acrylic acid). Previous work showed that chitosan-graft-poly(acrylic acid) superabsorbents improved water holding and retention in sandy soil, indicating their potential for agricultural moisture regulation [5].

Applied Science and Engineering Progress, Vol. 20, No. 4, 2027, 8324

For acrylic acid-based superabsorbents, alkaline saponification promotes sodium carboxylate formation and thereby increases water affinity, osmotic pressure, and electrostatic repulsion. Previous work on the same NaOH-saponified Cs-g-PAA formulations showed that saponification, acrylic acid neutralization, and nominal N,N′-methylenebisacrylamide (MBA) loading affected swelling, structural characteristics, and water retention. However, equilibrium capacity alone does not resolve the time-dependent contributions of water uptake and network rearrangement [6].

Kinetic modeling can quantify characteristic rates and provide model-dependent interpretations of swelling. Empirical models describe the overall profile, Ritger-Peppas is commonly used for an initial fractional-uptake region, and relaxation-based equations can indicate time-dependent network response. Such interpretations remain phenomenological unless supported by independent structural or rheological measurements. Machine-learning approaches have recently been explored for predicting hydrogel swelling behavior; however, their predictive performance depends on sufficiently rich datasets [7].

The present dataset contains only five formulations with ten time points per formulation, which is inadequate for robust model training and independent validation and would create a high risk of overfitting. Therefore, machine-learning or hybrid predictive modeling was not attempted in this study and is reserved for future work using larger, replicated, and independently validated datasets. The experimental swelling dataset analyzed here was previously reported by Jayanudin *et al.,* [6]; no new hydrogel synthesis or swelling measurements are claimed in the present manuscript. The additional contribution is a focused secondary kinetic analysis that applies several model classes to the same chitosan-graft-poly(acrylic acid) (Cs-g-PAA) formulations, clarifies the valid comparison domains of their statistics, and examines how the fitted parameters vary with neutralization degree and nominal MBA loading. The study therefore aims to provide a cautious, model-based interpretation of water uptake and possible network-relaxation effects while explicitly defining the limits of statistical discrimination and mechanistic inference.

2 Materials and methods

2.1 *Materials*

Acrylic acid (99%, CAS No. 79-10-7) and N,N′-methylenebisacrylamide (MBA, CAS No. 110-26-9) were purchased from Sigma-Aldrich, USA. Chitosan with a degree of deacetylation of 87.2% was supplied by PT. Biotech Surindo, Indonesia. Potassium hydroxide pellets (EMSURE®, CAS No. 1310-58-3) and ammonium persulfate (APS, CAS No. 7727-54-0) were obtained from Merck KGaA, Germany. Acetic acid, sodium hydroxide, and ethanol were obtained from Merck.

2.2 *Preparation of NaOH-saponified chitosan-graft-poly(acrylic acid) hydrogels*

The preparation procedure for the NaOH-saponified chitosan-graft-poly(acrylic acid) (Cs-g-PAA) superabsorbent hydrogels analyzed in the present study was previously reported by Jayanudin *et al.,* [6]. The synthesis procedure is summarized here only to provide the formulation and processing context required for interpretation of the secondary kinetic analysis; no new hydrogel synthesis was performed in the present study. The chitosan concentration was fixed at 4% (w/v) (Table 1). Acrylic acid was partially neutralized by dissolving 3.36, 4.48, and 5.60 g KOH in 100 mL distilled water to obtain 30%, 40%, and 50% neutralization degrees, respectively. Each KOH solution was added to 15 mL of acrylic acid and stirred for 15 min.

Table 1: Formulation variables and sample codes of NaOH-saponified Cs-g-PAA superabsorbent hydrogels.

Sample code	Chitosan Concentration (% w/v)	Acrylic acid neutralization degree (%)	MBA content (g)
Cs-g-PAA-1	4	30	0.050
Cs-g-PAA-2	4	40	0.050
Cs-g-PAA-3	4	50	0.050
Cs-g-PAA-4	4	50	0.015
Cs-g-PAA-5	4	50	0.100

A chitosan solution was prepared by dissolving 0.80 g chitosan in 20 mL of 2% (v/v) acetic acid, followed by the addition of 0.05 g APS dissolved in 5 mL of distilled water. The chitosan–APS solution was mixed with the partially neutralized acrylic acid solution and stirred for 30 min to initiate graft copolymerization. MBA was then added according to the formulation design: 0.050 g MBA for neutralization-degree variation at 30%, 40%, and 50%, and 0.015, 0.050, or 0.100 g MBA for crosslinker-

content variation at a fixed 50% neutralization degree. The mixture was stirred until gel formation occurred.

The formed hydrogel was saponified in 1 N NaOH at approximately 90 °C for 1 h to increase sodium carboxylate formation and hydrogel ionic character. The hydrogel was then filtered, washed with distilled water until neutral pH, dehydrated with ethanol, dried at 65 °C, and ground into powder to obtain NaOH-saponified Cs-g-PAA superabsorbent hydrogel.

2.3 *Swelling kinetic modeling*

The swelling data reanalyzed in the present study were obtained from the previously reported gravimetric measurements of Jayanudin *et al.,* [6]. In the original experiments, the swelling behavior of NaOH-saponified Cs-g-PAA superabsorbent hydrogels was evaluated in distilled water at 27 ± 1 °C using the tea-bag method. A known mass of dried hydrogel powder (W_d) was immersed in distilled water, and the swollen hydrogel mass (W_t) was recorded at 0, 5, 10, 20, 30, 60, 120, 240, 720, and 1440 min. No new swelling measurements were performed for the present secondary kinetic analysis. The swelling ratio at time t, S_t, was calculated using Eq. (1).

$$\text{Swelling ratio } (S_t)\left(\frac{g}{g}\right) = \frac{W_t - W_d}{W_d} \qquad (1)$$

where S_t is the swelling ratio at time t (g/g), W_t is the mass of the swollen superabsorbent at time t, and W_d is the initial dry mass of the hydrogel. The equilibrium swelling ratio, S_e, was determined when no significant change in swollen mass was observed with increasing swelling time.

2.4 *Fractional water uptake*

To compare water-transport profiles independently of equilibrium capacity, fractional uptake was calculated as $F_t = {S_t}/{S_e}$, where S_e was the experimentally observed plateau swelling ratio for each formulation. The same fixed S_e was used for normalization in the Ritger-Peppas analysis and as the scale linking fractional uptake to the swelling-ratio representation of the mixed model:

$$F_t = \frac{S_t}{S_e} \qquad (2)$$

where (F_t) is the fractional water uptake at time (t), (S_t) is the swelling ratio at time (t), and (S_e) is the equilibrium swelling ratio. This normalized parameter was used to compare the time-dependent water uptake behavior among formulations and to support the application of diffusional and mixed diffusion–relaxation models.

2.5 *Kinetic models for swelling and water transport*

The models were used for different analytical purposes. Schott, Peleg, Weibull, and Voigt described the complete swelling-ratio profile, S_t. Ritger-Peppas was used only for the initial fractional-uptake region ($F_t \leq 0.6$). The mixed diffusion-relaxation equation was used as a phenomenological two-component representation of the complete uptake curve; its fitted components were not interpreted as uniquely identifiable physical mechanisms.

2.5.1 Schott model

The Schott model was used to describe overall swelling behavior and estimate the theoretical equilibrium swelling capacity. Its nonlinear form is given in Eq. (3):

$$(S_t) = \frac{k_S S_e^2 t}{1 + k_S S_e t} \qquad (3)$$

where S_t is the swelling ratio at time t, S_e is the equilibrium swelling ratio, and k_S is the Schott swelling rate constant.

2.5.2 Peleg model

The Peleg model was used to describe water absorption behavior, particularly rapid initial swelling followed by gradual equilibrium. Its equation is given in Eq. (4):

$$(S_t) = \frac{t}{K_1 + K_2 t} \qquad (4)$$

where S_t is the swelling ratio at time t, K_1 is the Peleg rate constant, and K_2 is the Peleg capacity constant. The reciprocal of K_1 represents the initial swelling rate, while the reciprocal of K_2 is related to the theoretical equilibrium swelling capacity.

Applied Science and Engineering Progress, Vol. 20, No. 4, 2027, 8324

2.5.3 Weibull model

The Weibull model was employed to describe nonlinear swelling behavior over a broad swelling period and differences in apparent swelling-time distributions. The Weibull model is expressed as Eq. (5):

$$(S_t) = S_e\left(1 - \exp\left[-\left(\frac{t}{\alpha}\right)^{\beta}\right]\right) \quad (5)$$

where S_e is the equilibrium swelling ratio, α is the scale parameter associated with characteristic swelling time, and β is the shape parameter describing the swelling curve profile. A lower α value indicates faster characteristic swelling, whereas β reflects the deviation of swelling behavior from a simple first-order process.

2.5.4 Ritger–Peppas model

The Ritger–Peppas model was used to characterize the scaling of initial fractional water uptake without assigning a geometry-specific transport mechanism. The model is expressed as Eq. (6):

$$(F_t) = k_{R-P}t^n \quad (6)$$

where F_t is the fractional water uptake, k_{R-P} is a kinetic constant, and n is the empirical uptake exponent. Fitting was restricted to observations satisfying $F_t \leq 0.6$. Because the samples were powdered hydrogels with a particle-size distribution rather than an ideal slab, cylinder, or sphere, n was not assigned a strict geometry-specific Fickian classification ; it is reported only as a comparative initial-uptake exponent.

2.5.5 Voigt model

The Voigt model was used as a phenomenological relaxation-type representation of time-dependent swelling. In this framework, the fitted parameter τ is treated as an apparent response time rather than direct evidence of a viscoelastic relaxation constant. The model is expressed as Eq. (7):

$$(S_t) = S_e\left(1 - e^{-t/\tau}\right) \quad (7)$$

where S_t is the swelling ratio at time t, S_e is the equilibrium swelling ratio, and τ is an apparent response time. A lower τ value indicates a faster modeled approach to equilibrium, whereas a higher τ value indicates a slower modeled response. Without independent rheological measurements, this parameter is not assigned a unique viscoelastic mechanism.

2.5.6 Mixed diffusion–relaxation model

The mixed diffusion-relaxation equation was used as a two-component phenomenological model of the complete uptake curve. The fast and slow terms are denoted diffusion-like and relaxation-like for convenience, but their mathematical separation is not unique and does not constitute direct evidence of distinct physical processes. Fitted parameters are summarized in Table 2 [8].

The total fractional water uptake was expressed as the sum of diffusion and relaxation contributions :

$$F_t = F_F + F_R \quad (8)$$

$$\frac{dF_F}{dt} = k_F(\phi_F - F_F) \quad (9)$$

$$\frac{dF_R}{dt} = k_R(\phi_R - F_R) \quad (10)$$

Integration with the initial condition $F_F = F_R = 0$ at $t = 0$ yields

$$F_F = \phi_F[1 - exp\ (-k_F t)] \quad (11)$$

$$F_R = \phi_R[1 - exp\ (-k_R t)] \quad (12)$$

Thus, the mixed diffusion–relaxation model is expressed as:

$$F_t = \phi_F[1 - exp\ (-k_F t)] + \phi_R[1 - exp\ (-k_R t)] \quad (13)$$

where ϕ_F and ϕ_R are the fitted fractional amplitudes of the fast and slow components, and k_F and k_R are their respective apparent rate constants. Regression constraints were $0 \leq \phi_F, \phi_R \leq 1$, $\phi_F + \phi_R = 1$, and k_F, $k_R > 0$. S_E was fixed at the experimental plateau to reduce scale-parameter confounding. With only ten time points, the two exponential terms may be correlated; therefore, the parameters are exploratory descriptors rather than uniquely identifiable physical constants. Replicate-level data were unavailable for reliable confidence intervals, and this limitation precludes inferential comparisons among formulations.

2.6 *Model fitting, statistical evaluation, and model discrimination*

Nonlinear least-squares regression minimized residuals between experimental and calculated values. Whole-profile models used all ten observations, whereas Ritger-Peppas used only $F_t \leq 0.60$. R^2, SSE, RMSE, AIC, AICc, and BIC were treated as model-specific fit indicators. Direct ranking was permitted only when the response variable, observations, and error definition were identical; Ritger-Peppas was therefore excluded from whole-profile discrimination. The number of freely estimated parameters was $k = 2$ for Schott, Peleg, and Voigt, and $k = 3$ for Weibull and the two-component model because S_e was fixed and $\phi_R = 1 - \phi_F$. Equation (17) defines AIC, Equation (18) defines BIC, and Equation (19) defines AICc.

$$R^2 = 1 - \frac{\sum_{i=1}^{N}(S_{exp,i} - S_{cal,i})^2}{\sum_{i=1}^{N}(S_{exp,i} - \bar{S}_{exp})^2} \quad (14)$$

$$SSE = \sum_{i=1}^{N}\left(S_{exp,i} - S_{cal,i}\right)^2 \quad (15)$$

$$RMSE = \sqrt{\frac{1}{N}\sum_{i=1}^{N}\left(S_{exp,i} - S_{cal,i}\right)^2} \quad (16)$$

$$AIC = N \ln\left(\frac{SSE}{N}\right) + 2k \quad (17)$$

$$BIC = N \ln\left(\frac{SSE}{N}\right) + k \ln(N) \quad (18)$$

Because the whole-profile models were fitted using only $N = 10$ observations, the finite-sample correction of AIC was also calculated as

$$\text{AICc} = \text{AIC} + \frac{2k(k+1)}{N-k-1} \quad (19)$$

where $S_{exp,i}$ is the experimental swelling ratio, $S_{cal,i}$ is the calculated swelling ratio, $\bar{S}_{exp}$ is the average experimental swelling ratio, N is the number of experimental data points, and k is the number of free fitted parameters in each model. Because replicate-level observations and uncertainty propagation were unavailable, parameter differences are interpreted descriptively and not as statistically significant differences among formulations.

3 Results and Discussion

The reported swelling dataset was reanalyzed with complementary models. Statistical comparisons were restricted to compatible response scales and fitting ranges, while mechanistic statements were framed as model-based interpretations rather than direct experimental confirmation. The effects of MBA are discussed as effects of nominal crosslinker loading because crosslink density was not independently measured.

3.1 *Schott model*

The Schott model was applied to describe the swelling kinetics of NaOH-saponified Cs-g-PAA hydrogels based on pseudo-second-order behavior. The comparison between experimental and calculated swelling ratios is shown in Figure 1, and the corresponding equilibrium swelling capacity (S_e) and Schott rate constant (k_S) are summarized in Table 2. The Schott model described the swelling profiles well (R^2 = 0.977-0.997). The curves showed rapid initial uptake followed by a slower approach to equilibrium. Within this empirical framework, the response is consistent with rapid hydration followed by progressively restricted network expansion; however, the model alone does not identify the governing molecular mechanism.

The calculated equilibrium swelling capacity was influenced by neutralization degree and nominal MBA loading. At 0.050 g MBA, S_e increased from 165.55 g/g at 30% neutralization to 172.22 g/g at 40%,

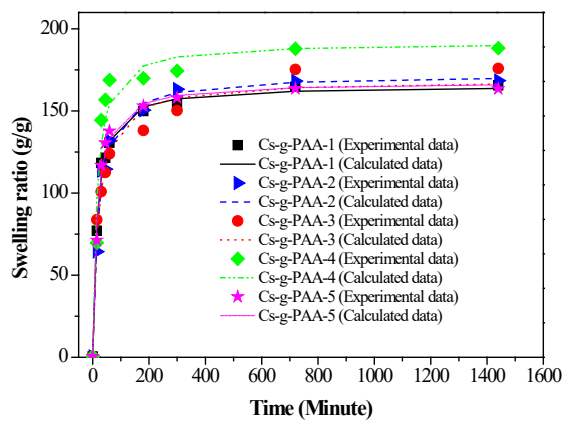

Figure 1: Comparison of experimental and calculated swelling ratios of NaOH-saponified chitosan-graft-poly(acrylic acid)-based superabsorbents using the Schott kinetic model.

then decreased slightly to 168.77 g/g at 50%. At 50% neutralization, Cs-g-PAA-4 (0.015 g MBA) showed the highest S_e (191.83 g/g), whereas Cs-g-PAA-5 (0.100 g MBA) reached 167.74 g/g. These trends are consistent with easier expansion at lower crosslinker loading, but they do not independently quantify crosslink density. The Schott rate constant ranged from 2.85 x 10^{-4} to 3.93 x 10^{-4} in the units defined by Eq. (3).

Based on RMSE, AIC, AICc, and BIC, the Schott fit ranked from lowest to highest error as Cs-g-PAA-1, Cs-g-PAA-5, Cs-g-PAA-2, Cs-g-PAA-3, and

Table 2: Kinetic parameters and coefficient of determination (R^2) of swelling models for NaOH-saponified Cs-g-PAA superabsorbent hydrogels.

Constant	Variable				
	Cs-g-PAA-1	**Cs-g-PAA-2**	**Cs-g-PAA-3**	**Cs-g-PAA-4**	**Cs-g-PAA-5**
Schott model					
S_e (g/g)	165.551	172.222	168.769	191.830	167.736
k_S [(g/g)$^{-1}$ min^{-1}]	0.000393	0.000285	0.000296	0.000358	0.000388
R^2	0.997	0.995	0.987	0.977	0.995
Voigt model					
S_e (g/g)	156.317	161.646	157.709	181.349	158.697
τ (min)	24.863	30.768	30.004	23.358	24.965
R^2	0.976	0.980	0.924	0.978	0.993
Ritger-Peppas model					
S_e (fixed, g/g)	165.605	168.469	175.949	188.276	163.459
k_{R-P} (min^{-n})	0.406	0.330	0.337	0.393	0.408
n	0.139	0.174	0.160	0.148	0.142
R^2	0.943	0.905	0.983	0.846	0.904
Weibull model					
S_e (g/g)	161.863	165.248	188.898	178.545	159.441
α (min)	25.224	32.401	64.455	23.459	24.864
β (-)	0.574	0.699	0.338	1.403	0.900
R^2	0.990	0.986	0.995	0.986	0.994
Peleg model					
K_1 [min/(g/g)]	0.107	0.113	0.179	0.085	0.082
K_2 [(g/g)$^{-1}$]	0.006	0.006	0.006	0.005	0.006
R^2	0.991	0.990	0.941	0.950	0.988
Mixed diffusion–relaxation model					
S_e (fixed, g/g)	165.605	168.469	175.949	188.276	163.459
k_F (min^{-1})	0.0655	0.0520	0.0907	0.0462	0.0489
k_R (min^{-1})	0.0048	0.0061	0.0040	0.0014	0.0043
ϕ_F (-)	0.746	0.719	0.595	0.926	0.871
ϕ_R (-)	0.254	0.281	0.405	0.073	0.129
R^2	0.997	0.992	0.997	0.981	0.998

Cs-g-PAA-4. Cs-g-PAA-4 had the highest swelling capacity but the largest Schott-model deviation, indicating that equilibrium extent and goodness of fit are distinct properties; this difference is not evidence of a lower crosslink density or a unique swelling mechanism.

Schott-type behavior can be associated with the balance between osmotic driving forces and resistance to network expansion. The formation of ionized carboxylate groups during saponification enhances water affinity and electrostatic repulsion, whereas increasing crosslinker loading can restrict network expansion [6], [9]. However, because crosslink density was not independently measured in the present study, these relationships should be regarded as formulation-based interpretations rather than direct evidence of differences in network crosslink density.

3.2 *Peleg model*

The Peleg model was used to describe the swelling kinetics of NaOH-saponified Cs-g-PAA hydrogels, particularly the rapid initial water uptake followed by gradual equilibrium. As shown in Figure 2 and Table 2, the model fitted the swelling profiles reasonably well, with R^2 values of 0.991, 0.990, 0.941, 0.950, and 0.988 for Cs-g-PAA-1 to Cs-g-PAA-5, respectively. Better agreement was observed for Cs-g-PAA-1, Cs-g-PAA-2, and Cs-g-PAA-5, while Cs-g-PAA-3 and Cs-g-PAA-4 showed lower fitting accuracy.

The Peleg constants describe the empirical initial uptake rate and theoretical equilibrium capacity. Based on $^1/_{K_1}$, Cs-g-PAA-5 and Cs-g-PAA-4 showed the fastest initial uptake, whereas Cs-g-PAA-3 showed the slowest. The highest theoretical equilibrium value was obtained for Cs-g-PAA-4 (190.46 g/g). This trend is associated with its lower nominal MBA loading, but does not independently quantify crosslink density.

Within the Peleg framework, Cs-g-PAA-1 showed the smallest error and Cs-g-PAA-4 the largest. The comparatively poorer fit for Cs-g-PAA-4 indicates that a single Peleg curve does not fully reproduce its profile; it is not, by itself, evidence of structural heterogeneity. Peleg parameters are therefore interpreted as empirical rate and capacity descriptors [10], [11].

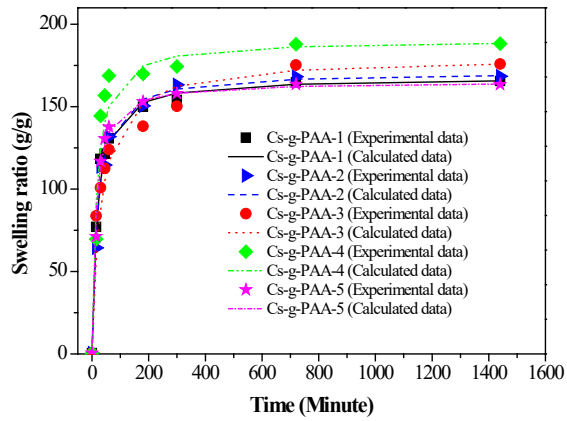

Figure 2: Peleg model fitting of swelling behavior for NaOH-saponified chitosan-graft-poly(acrylic acid)-based superabsorbents.

3.3 *Weibull model*

The Weibull model was used to describe nonlinear swelling behavior and differences in characteristic swelling time among NaOH-saponified Cs-g-PAA hydrogels. As shown in Figure 3 and Table 2, the model fitted all formulations well, with R^2 values of 0.990, 0.986, 0.995, 0.986, and 0.994 for Cs-g-PAA-1 to Cs-g-PAA-5, respectively. The calculated S_e values ranged from 159.44 to 188.90 g/g, confirming that swelling capacity was strongly influenced by acrylic acid neutralization degree and MBA crosslinker content.

The Weibull scale parameter ranged from 23.46 to 64.46 min. Lower values for Cs-g-PAA-4, Cs-g-PAA-5, and Cs-g-PAA-1 indicate shorter characteristic times within this empirical model. The shape parameter ranged from 0.3385 to 1.4027. Values below unity indicate a strongly decelerating profile, whereas the value above unity for Cs-g-PAA-4 indicates a different nonlinear curve shape. This behavior is consistent with a broader distribution of apparent swelling times but does not prove network heterogeneity without independent structural evidence. Within the Weibull model, Cs-g-PAA-3 and Cs-g-PAA-5 showed the smallest fitting errors, whereas Cs-g-PAA-4 showed the largest error among formulations. Across the compatible whole-profile models for Cs-g-PAA-4, however, Weibull produced the lowest reported error criteria. This distinction concerns the statistical description of the curve and is not independent proof of network heterogeneity. [12-16].

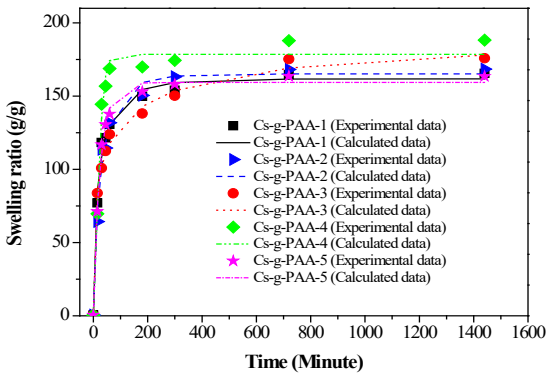

Figure 3: Weibull kinetic modeling of the swelling profiles of NaOH-saponified chitosan-graft-poly(acrylic acid)-based superabsorbents.

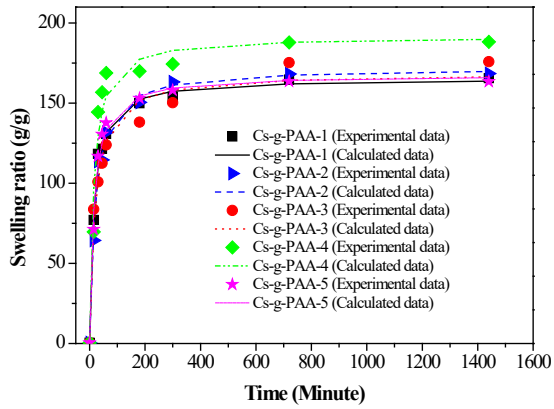

Figure 4: Voigt-model fitting of the time-dependent swelling response of NaOH-saponified chitosan-graft-poly(acrylic acid) superabsorbents.

3.4 *Ritger–Peppas model*

The Ritger-Peppas model was fitted only to the initial observations satisfying $F_t \leq 0.6$. The kinetic constant k ranged from 0.330 to 0.408, and the fitted exponent n ranged from 0.139 to 0.174 (Table 2). Because particle geometry and size distribution were not controlled to an ideal geometry, these n values are reported as comparative empirical exponents rather than classified as definitive Fickian or non-Fickian mechanisms.

R^2 ranged from 0.846 to 0.983. The lower fit quality for Cs-g-PAA-4 suggests that its initial uptake is not adequately summarized by a single power-law exponent over the selected range. The analysis does not establish a unique transport mechanism because the exponent depends on fitting range, sample geometry, and structural assumptions.

Ritger-Peppas was not included in whole-profile AIC/AICc/BIC discrimination because it used a different response scale and a restricted subset of observations. Its role is limited to comparative description of initial fractional uptake [16-19].

3.5 *Voigt model*

The Voigt model was used as a phenomenological representation of time-dependent swelling and possible network relaxation (Figure 4). The fitted equilibrium capacity (S_e) describes swelling extent, while τ is an apparent response time. A smaller tau corresponds to a faster modeled response.

In the absence of rheological measurements, Voigt fitting cannot confirm viscoelastic relaxation and is interpreted only as being consistent with a relaxation-like contribution.

Within the Voigt framework, Cs-g-PAA-5 showed the smallest error and Cs-g-PAA-3 the largest. The result indicates different apparent response times among formulations, but independent rheology would be required to verify viscoelastic relaxation [12], [20-22].

3.6 *Mixed diffusion–relaxation model*

The two-component model represented the swelling profile as apparent fast and slow uptake terms. Figure 5 compares experimental and calculated values, and Table 2 summarizes the fitted parameters. The labels are phenomenological and are not direct evidence of distinct molecular diffusion and polymer-relaxation processes. The two-component model showed high goodness of fit (R^2 = 0.981-0.998). The apparent fast rate constant, k_F, ranged from 0.0462 to 0.0907 min^{-1}, whereas k_R ranged from 0.0014 to 0.0061 min^{-1}. Cs-g-PAA-4 combined the highest equilibrium capacity with the lowest apparent rates. This is plausible because capacity describes the final extent of uptake, whereas the rate constants describe how rapidly that state is approached; a highly expandable network can therefore swell more extensively but more slowly.

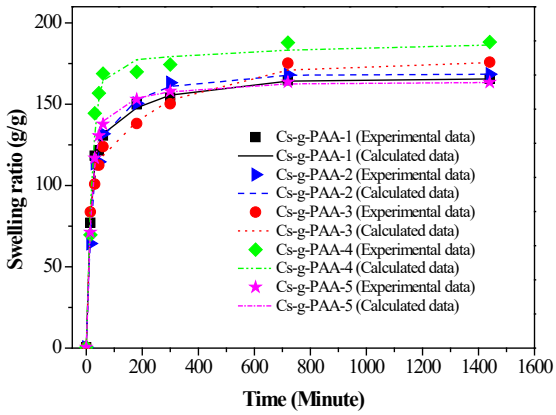

Figure 5: Comparison between experimental and calculated swelling ratios of NaOH-saponified Cs-g-PAA superabsorbent hydrogels using the mixed diffusion–relaxation model.

The fitted fast-component amplitude exceeded the slow-component amplitude for all formulations, indicating that the early term contributed most strongly within this equation. Because parameter correlation and non-uniqueness remain possible, ϕ_F and ϕ_R should not be interpreted as measured molecular fractions. Crosslink density, pore size, morphology, and rheology were not measured; correlations are therefore limited to neutralization degree and nominal MBA loading.

3.7 *Model fitting, statistical evaluation, and model discrimination*

Table 3 reports model-specific RMSE, AIC, AICc, and BIC values. Comparisons were restricted to fits with identical response variables, observations, and error definitions. Ritger-Peppas was excluded because it used only the initial $F_t \leq 0.60$ region. The results remain descriptive because only ten time points and no replicate-level uncertainty were available.

For Cs-g-PAA-1, Cs-g-PAA-3, and Cs-g-PAA-5, the mixed diffusion–relaxation model gave the lowest RMSE, AIC, AICc, and BIC values among the compatible whole-profile models. For Cs-g-PAA-4, the Weibull model consistently produced the lowest values for all four statistical criteria, indicating the best statistical description of its swelling profile within the models evaluated. Cs-g-PAA-2 showed a less uniform ranking: the mixed diffusion–relaxation model provided the lowest RMSE, AIC, and BIC values, whereas the Schott model yielded the lowest AICc value (35.550 compared with 37.022 for the mixed model). This difference arises from the stronger finite-sample penalty applied by AICc to models with more freely estimated parameters. Accordingly, no single model can be identified as uniformly superior for Cs-g-PAA-2 across all statistical criteria. These rankings describe goodness of fit and model parsimony only and do not establish network heterogeneity or uniquely distinguish molecular diffusion from polymer-relaxation processes. Given the small dataset, absence of replicate-level uncertainty, and possible parameter correlation, the model comparisons should be interpreted descriptively rather than as definitive mechanistic discrimination.

From a design perspective, within the investigated formulation window, lower nominal MBA loading favored higher equilibrium uptake but did not necessarily produce faster apparent kinetics. Accordingly, equilibrium swelling capacity and characteristic uptake time should be treated as separate design objectives when screening formulations for water-retention or controlled-release applications. These trends are specific to the investigated NaOH-saponified Cs-g-PAA formulations and should not be interpreted as universal predictive rules. Further predictive development requires independent measurements of crosslink density, pore structure, network morphology, and rheological properties, together with replicated swelling experiments across pH, ionic strength, salinity, and temperature. Repeated swelling–deswelling cycles and prolonged storage should also be evaluated to determine hydrogel durability and the stability of the fitted kinetic parameters. The parameters reported here are therefore limited to the investigated single-cycle swelling dataset. Furthermore, the present dataset is too small for defensible machine-learning or hybrid predictive modeling, which would require substantially larger, replicated, and independently validated datasets.

4 Conclusions

This secondary analysis is limited to NaOH-saponified Cs-g-PAA hydrogels measured in distilled water at 27 ± 1 °C. Neutralization degree and nominal MBA loading affected equilibrium capacity and apparent kinetic parameters. Cs-g-PAA-4 showed the

Table 3: Statistical evaluation and model discrimination of swelling kinetic models based on RMSE, AIC, AICc, and BIC values.

Constant	Variable				
	Cs-g-PAA-1	**Cs-g-PAA-2**	**Cs-g-PAA-3**	**Cs-g-PAA-4**	**Cs-g-PAA-5**
Schott model					
RMSE	3.864	5.246	8.331	12.848	5.060
AIC / AICc	28.329 / 30.044	33.836 / 35.550	42.159 / 43.873	49.957 / 51.672	33.183 / 34.898
BIC	28.724	34.230	42.553	50.352	33.578
Voigt model					
RMSE	7.742	7.560	14.130	8.921	4.203
AIC / AICc	40.841 / 42.555	40.413 / 42.127	51.669 / 53.384	43.392 / 45.106	29.845 / 31.559
BIC	41.235	40.807	52.064	43.786	30.239
Weibull model					
RMSE	5.092	6.180	3.740	7.138	3.943
AIC / AICc	35.299 / 39.299	38.782 / 42.782	29.743 / 33.743	41.377 / 45.377	30.694 / 34.694
BIC	35.890	39.374	30.335	41.969	31.286
Peleg model					
RMSE	4.836	5.329	12.406	13.356	5.539
AIC / AICc	32.371 / 34.085	34.117 / 35.831	49.327 / 51.041	50.656 / 52.370	34.814 / 36.528
BIC	32.765	34.511	49.721	51.050	35.208
Mixed diffusion–relaxation model					
RMSE	2.851	4.487	3.012	8.326	2.229
AIC / AICc	24.855 / 28.855	33.022 / 37.022	25.848 / 29.848	44.149 / 48.149	20.427 / 24.427
BIC	25.447	33.613	26.440	44.740	21.018

highest capacity despite the lowest fast and slow rate constants, confirming that swelling extent and swelling rate are distinct design attributes.

The models provided complementary, non-equivalent descriptions of the swelling behavior. Schott, Peleg, Weibull, and Voigt summarized the complete swelling profiles; Ritger-Peppas described only the initial fractional-uptake region; and the two-component equation represented apparent fast and slow uptake terms. Statistical comparisons were restricted to compatible datasets and response scales, with AICc included to account for the small sample size. The mixed diffusion–relaxation model gave the lowest RMSE, AIC, AICc, and BIC values for Cs-g-PAA-1, Cs-g-PAA-3, and Cs-g-PAA-5, whereas the Weibull model consistently gave the lowest values for Cs-g-PAA-4. For Cs-g-PAA-2, the mixed model gave the lowest RMSE, AIC, and BIC, while the Schott model gave the lowest AICc, indicating that model ranking for this formulation depends on the balance between fitting accuracy and finite-sample complexity penalization. These results support phenomenological differences in uptake timescales but do not directly confirm molecular diffusion, viscoelastic relaxation, crosslink density, or structural heterogeneity.

Acknowledgments

The authors acknowledge financial support from the Ministry of Higher Education, Science, and Technology of the Republic of Indonesia through the Master's Thesis

Research Grant (B/546.1/UN43.9/PT.00.03/2026), and thank the Department and Master's Program of Chemical Engineering for research facilities and technical support.

Author Contributions

D.P.: Data curation, Investigation, Methodology, Formal analysis, Writing – original draft; R.: Data curation, Investigation, Methodology; J.: Conceptualization, Methodology, Supervision, Writing – review & editing; E.Y.W.: Conceptualization, Formal analysis, Validation, Writing – review & editing; W.E.K.: Investigation, Data curation, Validation, Writing – review & editing; R.H.: Investigation, Validation, Writing – review & editing.

Conflicts of Interest

The authors declare no conflict of interest.

Declaration of generative AI and AI-assisted technologies in the writing process

The authors used ChatGPT solely for language refinement and to improve the readability of the manuscript.

References

[1] R. Michalik and I. Wandzik, "A mini-review on chitosan-based hydrogels with potential for sustainable agricultural applications," *Polymers*, vol. 12, no. 10, Art. no. 2425, Oct. 2020, doi: 10.3390/polym12102425.

[2] D. Venkatachalam and S. Kaliappa, "Superabsorbent polymers: A state-of-art review on their classification, synthesis, physicochemical properties, and applications," *Reviews in Chemical Engineering*, vol. 39, no. 1, pp. 127–171, 2023, doi: 10.1515/revce-2020-0102.

[3] M. Yang, J. Wu, G. M. Graham, J. Lin, and M. Huang, "Hotspots, frontiers, and emerging trends of superabsorbent polymer research: A comprehensive review," *Frontiers in Chemistry*, vol. 9, Art. no. 688127, Jul. 2021, doi: 10.3389/fchem.2021.688127.

[4] F. Hong, M. Zhang, C. Zhang, H. Chen, and Y. Liu, "Chitosan-based hydrogels: From preparation to applications, a review," *Food Chemistry: X*, vol. 21, Art. no. 101095, Mar. 2024, doi: 10.1016/j.fochx.2023.101095.

[5] Jayanudin et al., "Chitosan-graft-poly(acrylic acid) superabsorbent's water holding in sandy soils and its application in agriculture," *Polymers*, vol. 14, no. 23, Art. no. 5175, Nov. 2022, doi: 10.3390/polym14235175.

[6] Jayanudin et al, "Ion-responsive chitosan-graft-poly(acrylic acid) hydrogels via saponification: Structure, swelling kinetics, and water retention," *Polymer*, vol. 336, Art. no. 128930, Oct. 2025, doi: 10.1016/j.polymer.2025.128930.

[7] W. Zhang et al, "Factors affecting the properties of superabsorbent polymer hydrogels and methods to improve their performance: A review," *Journal of Materials Science*, vol. 56, no. 30, pp. 16223–16242, Oct. 2021, doi: 10.1007/s10853-021-06306-1.

[8] N. Yavari and S. Azizian, "Mixed diffusion and relaxation kinetics model for hydrogels swelling," *Journal of Molecular Liquids*, vol. 363, Art. no. 119861, Oct. 2022, doi: 10.1016/j.molliq.2022.119861.

[9] D. Salgado-Chavarría and J. Palacios-Alquisira, "Poly(vinyl alcohol) membranes cross-linked with maleic anhydride and 2,5-furandicarboxylic acid: Conventional heating and microwave irradiation," *ChemistrySelect*, vol. 5, no. 16, pp. 4826-4838, Apr. 2020, doi: 10.1002/slct.202000564.

[10] M. D. Ureña-Amate, M. del M. Socias-Viciana, M. del M. Urbano-Juan, and M. del C. García-Alcaraz, "Effects of pH and crosslinking agent in the evaluation of hydrogels as potential nitrate-controlled release systems," *Polymers*, vol. 15, no. 5, Art. no. 1246, Mar. 2023, doi: 10.3390/polym15051246.

[11] S. A. Dhahir, A. J. Braihi, and S. A. Habeeb, "Preparation and characterization of supramolecular bonding polymers based on a pullulan substrate grafted with acrylic acid/acrylamide by microwave irradiation," *ChemEngineering*, vol. 8, no. 4, Art. no. 77,Jul. 2024, doi: 10.3390/chemengineering8040077.

[12] J. Lee et al, "Preparation and characterization of superabsorbent polymers based on starch aldehydes and carboxymethyl cellulose," *Polymers*, vol. 10, no. 6, Art. no. 605, May 2018, doi: 10.3390/polym10060605.

[13] S. B. Shruthi, C. Bhat, S. P. Bhaskar, G. Preethi, and R. R. N. Sailaja, "Microwave assisted

synthesis of guar gum grafted acrylic acid/nanoclay superabsorbent composites and its use in crystal violet dye absorption," *Green and Sustainable Chemistry*, vol. 6, no. 1, pp. 11-25, Feb. 2016, doi: 10.4236/gsc.2016.61002.

[14] Y. Zhang, L. Zhao, K. Ma, and G. Z. Mao, "Synthesis and characterization of graft copolymers of acrylic acid onto starch," *Key Engineering Materials*, vol. 693, pp. 638–643, May 2016, doi: 10.4028/www.scientific.net/KEM.693.638.

[15] M. V. Uspenskaya, V. E. Sitnikova, M. A. Dovbeta, R. O. Olekhnovich, and I. Yu. Denisyuk, "Sorption properties of clay and pectin-containing hydrogels," in *Recent Research in Polymerization*, N. Cankaya, Ed. London, U.K.: IntechOpen, 2018, ch. 5, pp. 95–113, doi: 10.5772/intechopen.71190.

[16] S. M. Lalji, S. I. Ali, R. Ahmed, S. Hashmi, and Z. U. H. Awan, "Comparative performance analysis of different swelling kinetic models for the evaluation of shale swelling," *Journal of Petroleum Exploration and Production Technology*, vol. 12, no. 5, pp. 1237-1249, May 2022, doi: 10.1007/s13202-021-01387-9.

[17] E. Czarnecka and J. Nowaczyk, "Synthesis and characterization superabsorbent polymers made of starch, acrylic acid, acrylamide, poly(vinyl alcohol), 2-hydroxyethyl methacrylate, 2-acrylamido-2-methylpropane sulfonic acid," *International Journal of Molecular Sciences*, vol. 22, no. 9, Art. no. 4325, Apr. 2021, doi: 10.3390/ijms22094325.

[18] J. Kobryń, T. Zięba, S. K. Sowa, and W. Musiał, "Influence of acetylated annealed starch on the release of β-escin from the anionic and non-ionic hydrophilic gels," *Pharmaceutics*, vol. 12, no. 1, Art. no. 84, Jan. 2020, doi: 10.3390/pharmaceutics 12010084.

[19] H. Omidian, A. Akhzarmehr, and S. D. Chowdhury, "Advancements in cellulose-based superabsorbent hydrogels: Sustainable solutions across industries," *Gels*, vol. 10, no. 3, Art. no. 174, Mar. 2024, doi: 10.3390/gels10030174.

[20] X. Qi, M. Liu, and Z. Chen, "Fast-swelling oxidized starch phosphate-poly(acrylate/acrylamide/2-acryloylamino-2-methyl-1-propanesulfonic acid) superabsorbent composite," *Polymer Engineering & Science*, vol. 56, no. 11, pp. 1267-1274, Nov. 2016, doi: 10.1002/pen.24360

[21] H. Tian, S. Cheng, J. Zhen, and Z. Lei, "Superabsorbent polymer with excellent water/salt absorbency and water retention, and fast swelling properties for preventing soil water evaporation," *Journal of Polymers and the Environment*, vol. 31, no. 2, pp. 812-824, Feb. 2023, doi: 10.1007/s10924-022-02543-w.

[22] M. Chen et al, "Kaolin-enhanced superabsorbent composites: Synthesis, characterization and swelling behaviors," *Polymers*, vol. 13, no. 7, Art. no. 1204, Apr. 2021, doi: 10.3390/polym13071204.